Study on the Cold Forming Effect on in Cold rolled Austenitic Stainless Steel Hollow Sections

Baofeng Zheng[a], Qinglin Jiang[b], Jin Chen[c] and Ganping Shu[a]

School of Civil Engineering, Southeast University, Nanjing, China[(a)]
Jiangsu Dongge Stainless Steel Ware Co., Ltd, Jiangsu, Dongtai, China[(b)]
Nanjing Architectural Design & Research Institute Co., Nanjing Ltd[(c)]

Abstract

The cold forming effect on cold rolled austenitic stainless steel tubes was investigated in this study through a test programme in a series of test specimens including four rectangular hollow sections and four circular hollow sections. Residual stresses in cold rolled tubes were measured using a modified sectioning method with the results indicating that the longitudinal bending residual stresses were the dominant component. Residual stress distribution models were proposed for rectangular and circular hollow sections, respectively based on the test results. Material tensile tests were performed for both the cold rolled tubes and the virgin plates and the results show that the material stress was considerably enhanced during the cold rolling process with the improvement level dependent on the type of cross section and the position in the cross section. A new material model for the cold rolled tube was proposed based on material parameters of virgin plate and equivalent strain. The proposed model indicates good accuracy in predicting the strength enhancement through comparison with the test results.

Keywords

Stainless steel, Cold-rolling, Rectangular hollow section, Circular hollow section, Residual stresses, Strength enhancement.

1 Introduction

Stainless steel has become an attractive material in building constructions due to its durability, favourable mechanical properties and aesthetic appearance. Austenitic stainless steel is the most commonly used stainless steel in construction work while the high initial cost of material is still a biggest obstacle in promoting the application of stainless steel structures. Cold forming effect e.g. residual stresses and material enhancement has been proved by many researchers and could be considered in the design of cold rolled stainless steel members to fully exploit material properties and to reduce the construction cost.

Cold forming effect of stainless steel members has been studied including residual stresses [1-10] and material enhancement[11-18]. Residual stress model for stainless steel rectangular hollow sections has been proposed [6][8], but not for the circular hollow sections. Material enhancement model has been proposed for the nominal yield stress [13][14][15][17] and the ultimate tensile stress [13][14][15], but not for other parameters such as strain hardening exponent and ultimate tensile strain, etc.

Cold rolling is an efficiency cold forming process in producing small to medium stainless steel tubes and has been widely used in China. The main purpose of this study is to investigate the cold forming effect of the cold rolled austenitic stainless steel tubes through experimental study and to develop the distribution model of residual stresses and the prediction models for all material parameters.

2 Test Program

Test program consisted of two parts: measurement of residual stresses and material tensile tests. The test specimens were cold-rolled from austenitic stainless steel plate of S30408 and consist of eight types of cross sections. The nominal cross-sections of the rectangular hollow sections (RHS) were 100mm×100mm×3mm, 70mm×70mm×3mm, 100mm×50mm×3mm and 40mm×40mm×2mm. The nominal cross-sections of the circular hollow sections (CHS) were 127mm×3mm, 89mm×3mm, 96mm×3mm and 50.8mm×2mm. The RHS was processed by rolling the plate into a CHS first and then crushing into a RHS. All specimens were in cold formed state without the annealing process.

2.1 Measurement of residual stresses

Sectioning method is a common method for the measurement of residual stresses in built-up stainless steel sections [19-21]. The main procedures involve drilling holes sequentially cutting out part of the specimen and measuring the change in the distance between the holes using Whittemore gauge. This method is suitable for members in which the longitudinal membrane stresses were dominant [22]. The method is improper for cold formed stainless steel members since the transverse and the longitudinal bending residual stresses were the major stresses due to the extensive plastic deformation in both the transverse and longitudinal directions [23]. In this study, the traditional sectioning method was modified by replacing the Whittemore gauge with strain gauges to measure the released strain during cutting process. Since the residual stresses in the cold formed sections were approximately in the plane stress state, strain gauge (BX120-2BB) of T rosettes

Paper presented by Baofeng Zheng - zhengbaofeng2000@sina.com

with two measuring grids offset by 90 degree and three solder tabs was used as illustrated in Fig.1. The nominal electric resistance was 120 Ohm with active measured grid length 2mm×2mm.

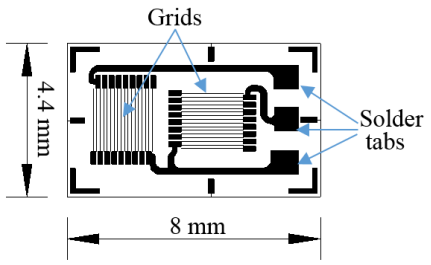

Fig. 1 T rosettes with three solder tabs (BX120-2BB)

Strain gauges were attached onto the inner and the outer surfaces of the hollow sections using the cyanoacrylate glue and covered by silicon rubber for electric isolation. No strain gauge was installed on the inner surface of the corner regions of RHS due to the physical limitation.

The width of the strip was varied from 8mm to 10mm considering the size of the strain gauge, the rubber cover and the cross section. The strips were evenly distributed across the cross-section. The number of strips was 18 for the sections CHS 127 mm × 3 mm, CHS 89 mm × 3 mm and CHS 96 mm×3 mm; 8 for CHS 50.8 mm × 2 mm; 40 for RHS 100 mm × 100 mm × 3 mm; 32 for RHS 70 mm × 70 mm × 3 mm; 28 for RHS 100 mm × 50 mm × 3 mm; and 16 for RHS 40 mm × 40 mm × 2 mm with the total number reaching 160.

The length of strips was set as 150 mm. The cutting region was located at the centre of the specimen. The total length of the specimen was designed as the two times of the section height (diameter) plus the length of the strips to retain the residual stress field [24].

To minimize the interaction among the strips when cutting one of them, three specimens were used for CHS and five for RHS. Typical strip arrangements for RHS 100 mm × 100 mm × 3 mm and CHS 127 mm × 3 mm are shown in Fig.2 and Fig.3, respectively. During the cutting stage, strain changes in adjacent strips were also monitored for further analysis. For example, when cutting the strips 2 and 30 of RHS 100 mm × 100 mm × 3mm (Specimen A), the strain changes of strips 4 and 28 were also recorded.

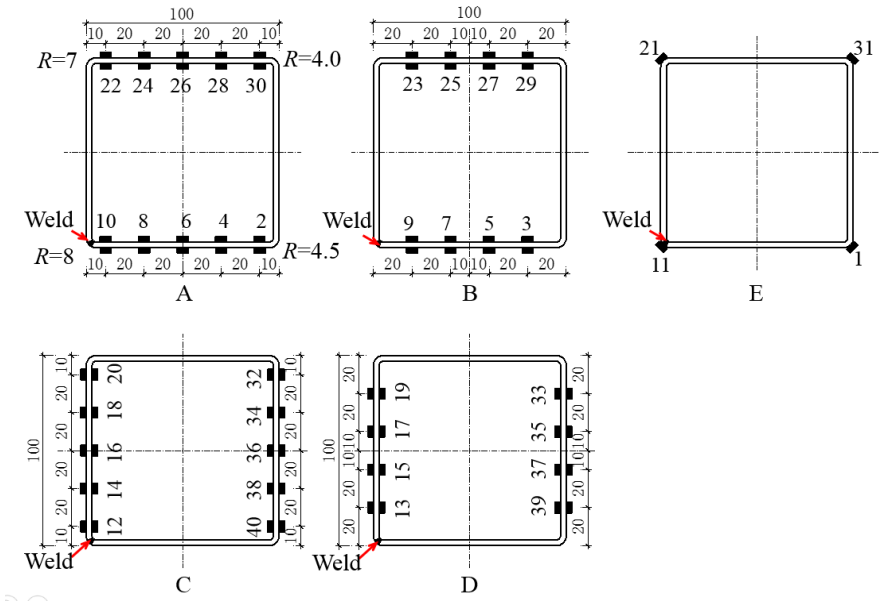

Fig. 2 Test point arrangement for RHS 100mm×100mm×3mm

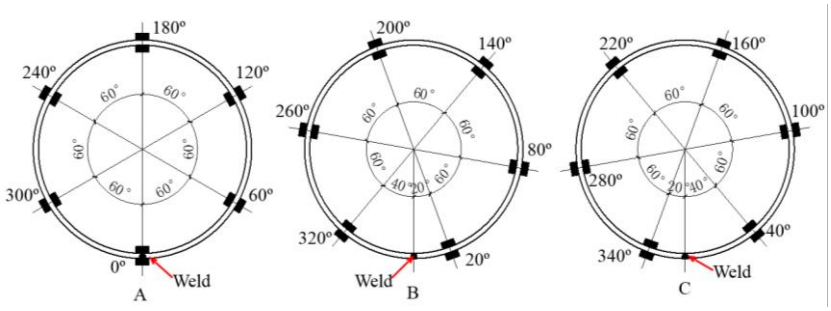

Fig. 3 Test point arrangements for CHS 127mm×3mm

Cutting operation was performed using an automatic electric spark wire cutting machine with minimal heat input into strips. The cutting duration for one pair of strips lasted for approximately 30 minutes with the time history of released strain recorded by the data acquisition system TDS303. Test instrument layout is shown in Fig.4.

Fig. 4 Test rig for measurement of residual stresses

2.2 Residual stresses data processing

Residual strains on both surfaces in the longitudinal and the transverse directions were obtained for every strip. Based on the plane stress assumption, the residual stresses in the longitudinal and the transverse directions can be calculated using Eq. (1).

$$\begin{cases} \sigma_{\mathrm{L,o(i)}} = \dfrac{E}{1-v^2}\left(\varepsilon_{\mathrm{L,o(i)}} + v\varepsilon_{\mathrm{T,o(i)}}\right) \\ \sigma_{\mathrm{T,o(i)}} = \dfrac{E}{1-v^2}\left(\varepsilon_{\mathrm{T,o(i)}} + v\varepsilon_{\mathrm{L,o(i)}}\right) \end{cases} \tag{1}$$

where, E is the elastic modulus; v is the possion ratio; $\varepsilon_{\mathrm{L,o}}$ and $\varepsilon_{\mathrm{L,i}}$ are the strain released in the longitudinal direction on the outer and the inner surfaces, respectively; $\varepsilon_{\mathrm{T,o}}$ and $\varepsilon_{\mathrm{T,i}}$ are the strain released in the transverse direction on the outer and the inner surfaces, respectively; $\sigma_{\mathrm{L,o}}$ and $\sigma_{\mathrm{L,i}}$ are the longitudinal stress on the outer and the inner surfaces, respectively; $\sigma_{\mathrm{T,o}}$ and $\sigma_{\mathrm{T,i}}$ are the transverse stress on the outer and the inner surfaces, respectively.

For the strips in corner regions, only the residual strain on the outer surface was measured. Thus, the pure bending state was assumed for corners. It means that the magnitude of $\varepsilon_{\mathrm{L,i}}$ equals to $\varepsilon_{\mathrm{L,o}}$ with an opposite sign.

Assumed that the residual stresses have a rectangular stress block distribution through thickness direction, the longitudinal and the transverse membrane and bending residual stresses can be calculate using Eq. (2).

$$\begin{cases} \sigma_{\mathrm{L(T),m}} = \dfrac{1}{2}\left(\sigma_{\mathrm{L(T),o}} + \sigma_{\mathrm{L(T),i}}\right) \\ \sigma_{\mathrm{L(T),b}} = \dfrac{1}{3}\left(\sigma_{\mathrm{L(T),o}} - \sigma_{\mathrm{L(T),i}}\right) \end{cases} \tag{2}$$

where, $\sigma_{\mathrm{L,m}}$ and $\sigma_{\mathrm{L,b}}$ are the longitudinal membrane and bending stress, respectively; $\sigma_{\mathrm{T,m}}$ and $\sigma_{\mathrm{T,b}}$ are the transverse membrane and bending stress, respectively.

Typical test results for RHS 100×100×3mm and CHS 127×3 mm are shown in Fig.7 (a) and Fig.7 (b), respectively. The horizontal axis in Fig.7 (b) was referred to the angle relative to the weld point.

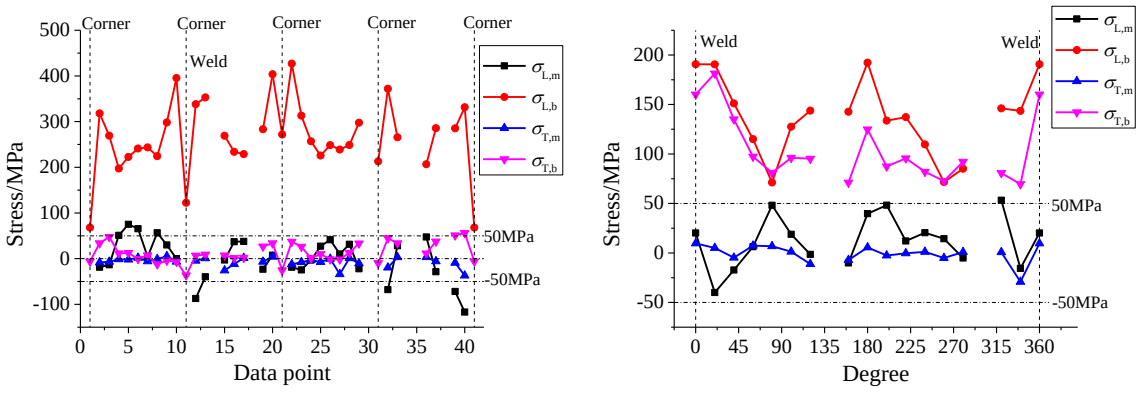

(a) RHS 100×100×3 **(b)CHS 127×3**

Fig. 5 Typical residual stresses test results

Fig.7 (a) indicates that: (1) compared with the longitudinal bending residual stresses, other three types of residual stress were much lower with the magnitude less than 50MPa. No clear distribution pattern was observed for these three types of residual stresses. (2) The longitudinal bending residual stresses were positive indicating that the outer surface of the section was in tension. (3) The longitudinal bending residual stresses were lower in the centre of the flat face, and grew dramatically from the centre to the intersection point of the flat face and the corner followed by a sharp drop appeared in the corner. (4) The position of weld is shown in this figure. No clear difference was shown between regions around the weld and the others.

Fig. 7(b) demonstrates that: (1) the longitudinal and the transverse membrane residual stresses were lower than 50MPa indicating no clear distribution pattern. (2) The longitudinal bending residual stresses had a 'W' type distribution pattern. The residual stresses at the degrees from 90 to 270 were lower than that at other regions while the high values occur at the regions around the weld and around 180 degree. (3) The transverse bending residual stresses were approximately evenly distributed along the cross section. Due to the complex stress state at the weld, the transverse residual bending stresses around the weld were a little higher than that at other regions.

2.3 Material tensile tests

Material tensile tests includes two parts: tests on the coupons from cold rolled tubes, and tests on the coupons from virgin plates. The coupons from cold rolled tubes came from the strips in the residual stress tests and 94 strips were used.. For example, for RHS 100mm×100mm×3mm, the strips from specimen A, C and E were tested. For CHS 127mm×3mm, strips from specimen A were tested. The coupons from virgin plates were obtained from the coil in the production lines. The RHS 100 mm × 100 mm × 3 mm members and CHS 127 mm × 3 mm members were formed in the same production line differed only in the last reshaping roll. Thus, only one virgin plate (G4) was obtained for RHS 100 mm × 100 mm × 3 mm and CHS 127 mm × 3 mm. The same situation applied for RHS 100 mm × 50 mm × 3 mm and CHS 96 mm × 3 mm (G3), RHS 70 mm × 70 mm × 3 mm and CHS 89 mm × 3 mm (G2), and RHS 40 mm × 40 mm × 2 mm and CHS 50.8 mm × 2 mm (G1). For every virgin plate, 9 coupons were extracted in three directions: longitudinal direction, transverse direction and 45 degree direction. Totally, 36 coupons from virgin plates were used in material tensile test.

Material tensile tests were performed in a 100 kN SANS universal testing machine in accordance with the Chinese standard GB/T 228.1-2010 [25]. The gauge length of the coupons was 50mm and the load rate was about 0.5 mm/min before the strain reached 0.02 and 5mm/min afterwards. Prior to testing, a pair of strain gauges were attached on each face of the coupon to obtain the strain-stress curve. To get rid of introducing the bending moment to the corner coupons, a pair of corner coupons were gripped symmetrically around the steel bar located at the end with the same radius as the corner in the test specimens.

Material test results were processed according to the two-stage strain-stress model [12]. The average results of the material test for virgin plates are shown in Table 1. The coupon names G4-Long, G4-Diag and G4-Trans indicate average result for coupons in the longitude, 45 degree, and transverse direction, respectively. Typical test results for CHS127 mm × 3 mm and RHS 100 mm × 100 mm × 3 mm are indicated in Table 2 and Table 3, respectively. The test coupons were labelled to demonstrate the cross-section and the position. For example, the label "M120×3-60" indicates the coupon for material test (M) from the cross-section CHS 120mm×3mm at the position 60 degrees away from weld (Fig.3). In these tables, E_0 is the material Young's modulus, $\sigma_{0.2}$ is the material 0.2% proof stress, n is a strain hardening exponent, $\sigma_{1.0}$ is the material 1.0% proof stress, $n_{0.2,1.0}$ is a strain hardening exponent representing a curve that passes through 0.2 and 1.0, σ_u is the ultimate tensile stress, δ is the percentage elongation after fracture, n_1, p and q are the parameters for the new material model proposed in this paper.

Table 1 Average material tensile test results for virgin plate G4 (CHS127mm×3mm and RHS100mm×100mm×3mm)

Coupons	E_0/MPa	$\sigma_{0.2}$/MPa	$\sigma_{1.0}$/MPa	σ_u/MPa	n	$n_{0.2,1.0}$	δ	n_1	q	p/MPa
G4-Long	187566	231.78	279.35	627.61	4.97	2.11	0.63	8.62	4.95	689.06
G4-Diag	190186	239.60	289.73	619.21	5.24	2.31	0.65	8.47	5.31	671.54
G4-Trans	205396	247.94	296.27	647.70	7.91	2.42	0.62	9.04	5.10	711.29

Table 2 Material tensile test results for CHS127mm×3mm

Coupons	E_0/MPa	$\sigma_{0.2}$/MPa	$\sigma_{1.0}$/MPa	σ_u/MPa	n	$n_{0.2,1.0}$	δ	n_1	q	p/MPa
M127×3-0	204044	414.27	467.39	-	5.39	3.03	0.46	13.34	-	-
M127×3-60	194217	287.20	335.08	640.54	6.13	2.46	0.62	10.44	6.12	692.55
M127×3-120	206079	297.43	344.83	647.80	5.41	2.50	0.64	10.88	6.35	694.96
M127×3-180	211941	350.06	395.10	-	5.59	2.63	0.62	13.30	-	-
M127×3-240	200910	319.41	363.32	654.97	8.12	2.59	0.64	12.49	6.78	699.57
M127×3-300	201927	305.78	349.32	650.45	6.67	2.47	0.60	12.09	6.33	705.12
Avg.	203186	329.02	375.84	648.44	6.22	2.61	0.60	12.10	7.19	696.76

Table 3 Material tensile test results for RHS100mm×100mm×3mm

Coupons	E_0/MPa	$\sigma_{0.2}$/MPa	$\sigma_{1.0}$/MPa	σ_u/MPa	n	$n_{0.2,1.0}$	δ	n_1	q	p/MPa
M100×3-2	182095	465.26	549.78	732.50	3.88	3.82	0.44	9.64	12.27	783.20
M100×3-4	188929	357.93	407.46	674.50	5.44	2.98	0.60	12.42	7.74	720.54
M100×3-6	198916	360.36	410.35	666.48	5.40	3.43	0.59	12.39	8.02	711.80
M100×3-8	225582	371.68	434.43	666.45	3.73	4.09	0.50	10.32	8.73	721.52
M100×3-10	184934	481.32	606.41	763.59	3.03	4.89	0.43	6.97	15.09	807.52
M100×3-12	188354	470.78	574.14	732.02	3.27	4.43	0.45	8.11	14.57	773.25
M100×3-14	193729	428.15	486.74	-	4.88	3.83	-	12.55	-	-
M100×3-16	189453	368.52	418.78	671.45	5.40	3.04	0.59	12.59	8.21	716.00
M100×3-18	188881	356.51	408.23	-	5.19	3.21	-	11.88	-	-
M100×3-20	176363	479.94	599.84	758.45	3.00	4.24	0.44	7.22	14.88	801.47
M100×3-22	208098	441.87	590.13	739.28	2.29	4.16	0.40	5.56	15.26	785.02
M100×3-24	193721	373.62	424.82	689.24	4.73	3.03	0.56	12.53	7.91	741.67
M100X3-26	209522	354.23	408.22	668.33	4.24	3.32	0.60	11.35	7.94	712.71
M100×3-28	194737	380.66	434.44	682.78	4.47	3.57	0.56	12.18	8.46	731.22
M100×3-30	198280	467.55	610.81	779.46	2.57	4.00	0.44	6.02	14.42	825.12
M100×3-32	182279	485.74	608.33	761.83	3.03	4.07	0.40	7.15	15.11	809.45
M100×3-34	188880	352.22	401.14	-	4.94	3.00	-	12.38	-	-

M100×3-36	193885	349.42	396.47	673.16	5.71	2.93	0.62	12.74	7.44	717.81
M100×3-38	190828	361.72	414.89	-	4.99	3.04	-	11.74	-	-
M100×3-40	184445	457.93	560.84	739.83	3.23	4.41	0.41	7.94	12.45	794.76
Avg.	193096	408.27	487.31	712.46	4.17	3.67	0.50	9.09	9.71	764.86
MC100×3-1	185007	468.93	557.52	760.08	4.98	3.53	0.46	9.30	11.50	813.16
MC100×3-2	204174	652.32	801.39	885.60	4.00	3.93	0.16	7.82	24.43	954.58
Avg.	194591	560.63	679.45	822.84	4.49	3.73	0.31	8.37	16.38	883.84

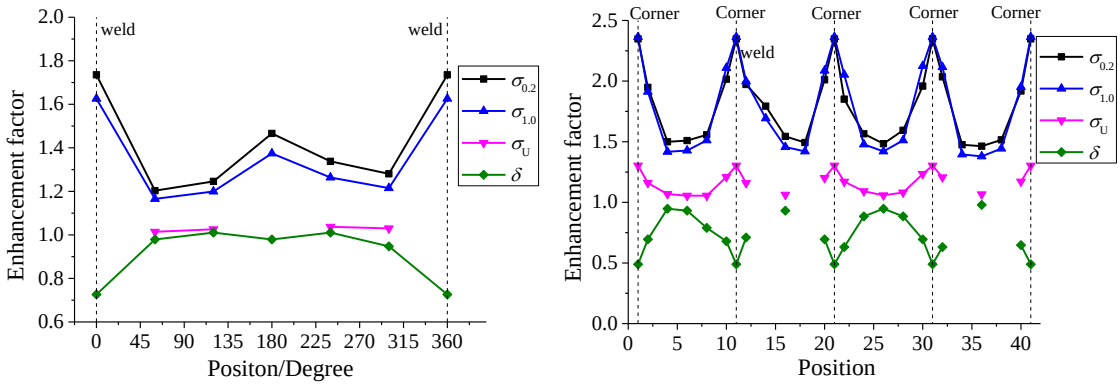

(a) CHS127mm×3mm (b) RHS100mm×100mm×3mm

Fig. 6

Material parameters of cold rolled tube normalized by those of virgin plate

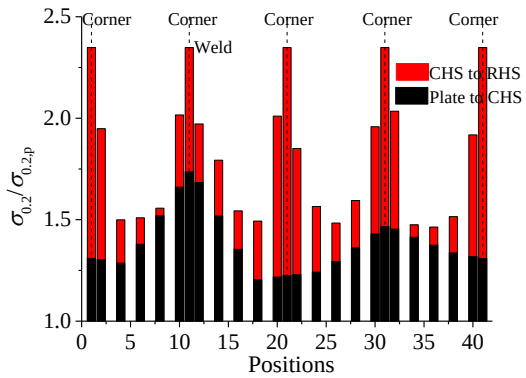

Fig. 7 Comparison of the yield stress increase during rolling to a CHS with that during crushing into a RHS

In Table 1, the values of each material parameters in three directions were similar. The yield strength in transverse direction (G4-Trans, 247.94 MPa) was only 7% higher than that in the longitudinal direction (G4-Long, 231.78 MPa). Thus, austenitic stainless steel in the annealed condition can be regarded as isotropic material.

Table 2 indicates that: (1) the nominal yield strength of M120×3-0 was 414.27 MPa, much higher than that of other coupons, while the elongation percentage was lower than that of other coupons. M120×3-0 located on the weld of the tube has the strength effected by the weld material. (2) Comparisons of the average material parameters of the tube (last row in Table 1) with those of the virgin material show that the material strength parameters, including $\sigma_{0.2}$ and $\sigma_{1.0}$, were enhanced in a large degree during the cold rolling process, while the other parameters have small changes. (3) The ratios of the material properties ($\sigma_{0.2}$, $\sigma_{1.0}$, σ_U, and δ) of the tube to those of the virgin plate are shown in Fig. 4(a). The lines for $\sigma_{0.2}$ and $\sigma_{1.0}$ have the similar trend, higher around the weld. The lines for σ_U and δ lies around 1.0 in most of the points.

Table 3 shows that: (1) Comparisons of the material strength parameters ($\sigma_{0.2}$, $\sigma_{1.0}$, and σ_U) of the coupon M100×3-6 with those of the coupon M100×30-10 show that material strength parameters in the centre of the flat face were lower than those of the edge of the flat face. The elongation percentage of M100×3-6 is 0.59, higher than that of M100×3-10. It means that the points of the flat face experienced different degrees of cold work. The experienced degree of cold work

increased from the center of the flat face to the corner of the tube. (2) The average nominal yield strength ($\sigma_{0.2}$ at the 4th row from the end) is 408.27 MPa that is about 1.76 times of that of the virgin plate.

The ratios of the material properties ($\sigma_{0.2}$, $\sigma_{1.0}$, σ_U, and δ) of the RHS to those of the virgin plate are shown in Fig. 4(b). It is clear that the lines for$\sigma_{0.2}$ and $\sigma_{1.0}$ have the similar trend. The ratio of the nominal yield stress of RHS to that of the virgin plate is up to 2.5 at the corner and decreases continually to 1.5 at the centre of the flat face. The line for the ultimate stress σ_U lies below the line for the nominal yield strength $\sigma_{0.2}$, which means the ultimate stress σ_U is not so sensitive to cold working than the nominal yield stress $\sigma_{0.2}$. The line for the percentage elongation δ shows opposite trend to the line for the ultimate stress σ_U. The higher the ultimate stress σ_U, the lower the percentage elongation δ.

The increase of the nominal yield stress during forming a CHS and during crushing into a RHS are compared in Fig.7. It can be seen that: (1) For the central part of flat region of the RHS, the yield stress increase during forming a CHS was higher than that during crushing into a RHS, while for the corner region and the adjacent flat region in the RHS, the yield stress increase during forming a CHS was lower than that during crushing into a RHS.

3 Residual Stresses Distribution Model

For RHS, only the longitudinal bending residual stresses were considered whereas the other three types of residual stresses were negligible. To develop a distribution model, the longitudinal bending residual stresses were firstly normalized using the material yield stress ($\sigma_{0.2}$ in Table 3) and the positions of test point on the flat face were normalized using the width of the cross section. The overall mean residual stresses values for the flat faces and the corners, together with the mean ± 1.64 standard deviations (representing the 95% percentile values based on a normal distribution) are indicated in Fig.8.

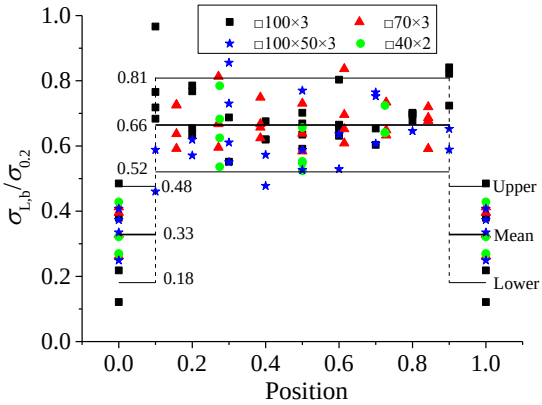

Fig. 8 Nominalised longitudinal bending residual stresses in RHS

The normalized longitudinal bending residual stresses in the cold rolled rectangular sections show a consistent tendency of tension at the outer surface of the section. The mean of the normalized bending residual stresses was higher in the flat regions of the sections and generally lower in the corner regions. The mean longitudinal bending residual stresses in the flat faces and the corners were $0.66\sigma_{0.2}$ and $0.33\sigma_{0.2,c}$, respectively. The upper values (mean + 1.64 standard deviations) were $0.81\sigma_{0.2}$ and $0.48\sigma_{0.2,c}$ for the flat faces and the corners, respectively, and the lower values were $0.52\sigma_{0.2}$ and $0.18\sigma_{0.2,c}$, respectively. A simple model for longitudinal bending residual stresses is given in Fig.10. The proposed model is very similar to the one proposed by in Ref.[6] with the difference in magnitudes.

For CHS, both the longitudinal and the transverse bending residual stresses are considered. The longitudinal bending residual stresses were firstly normalized by the nominal yield stress ($\sigma_{0.2}$ in Table 2) shown in Fig. 9(a) with an apparent "W" pattern. The red line "Test Avg." denotes the mean value at every individual degree. The higher residual stresses occur at the regions within degrees [0, 45], [135, 225] and [315, 360]whereas the minimum value of the residual stress was located at 90 degree and 270 degree away from the weld. The mean and the deviation for the regions within degrees [0, 45], [135, 225], and [315, 360] were $0.64\sigma_{0.2}$ and $0.14\sigma_{0.2}$, respectively. The mean residual stresses at the degrees 90 and 270 were $0.30\sigma_{0.2}$. A "W" types distribution model for the longitudinal bending residual stresses was proposed indicating in Fig.11(a).

The transverse bending residual stresses were assumed to be evenly distributed along the cross section. The residual stresses were normalized using material yield stress ($\sigma_{0.2}$ in Table 2). The overall mean residual stresses values for the transverse bending residual stresses, together with the mean ± 1.64 standard deviations are indicated in Fig.9 (b). The overall mean value and deviation were $0.31\sigma_{0.2}$ and $0.12\sigma_{0.2}$, respectively. A uniformed distribution model for the transverse bending residual stresses was proposed in Fig.11 (b).

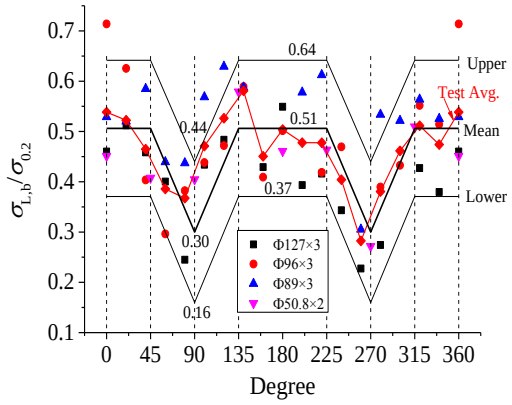

(a) Transverse bending

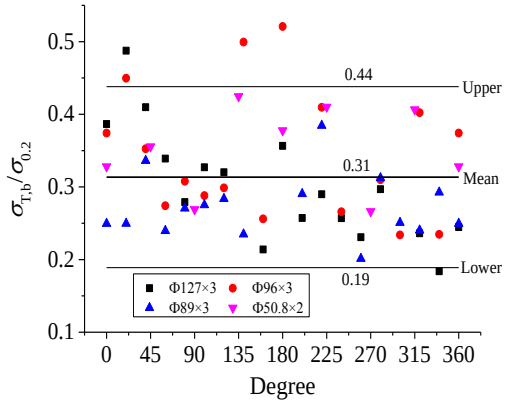

(b) Longitudinal bending

Fig. 9 Nominalised residual stresses in CHS

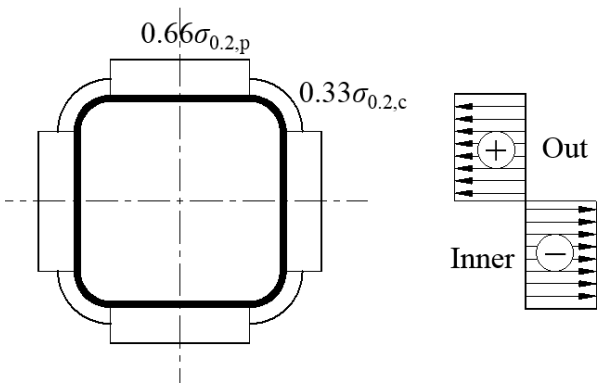

Fig. 10 Proposed longitudinal bending residual stress distribution model for RHS

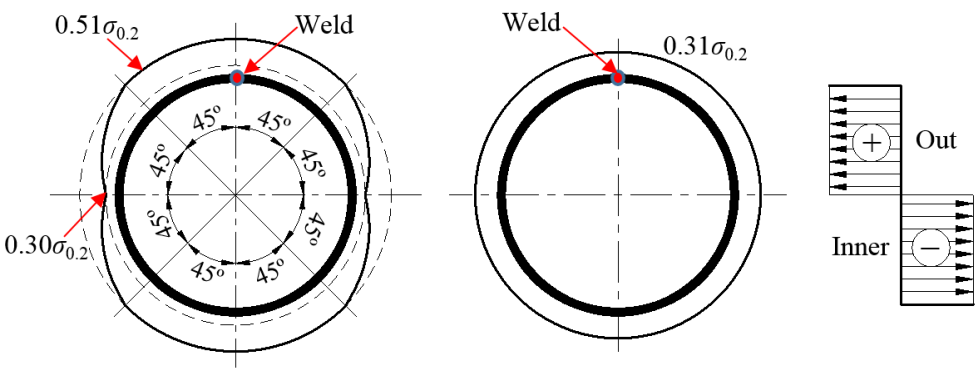

(a) Longitudinal bending **(b) Transverse bending**

Fig. 11 Proposed residual stress distribution model for CHS

4 Strength Enhancement Model

In this section, a new material model with less parameters was firstly proposed based on the material parameters of virgin plate and equivalent strain.

4.1 Material stress-strain model

Material model for stainless steel has been investigated by many researchers [12, 26-30]. Classical one-stage [26, 27], two-stage[12, 28-30] and three-stage [31] model have been proved to be accurate in certain strain range. This study was not targeted at a more accurate material model, but a model with acceptable accuracy and concise parameters. The proposed model consists of three stages: the first stage [0, $\sigma_{0.2}$] and the second stage [$\sigma_{0.2}$, $\sigma_{1.0}$] was in the form of Ramberg-Osgood function with different exponents while the third stage was a power function with the stress ranging from $\sigma_{1.0}$ to σ_U. This model is shown in Eq.(3) and Eq.(4). including six parameters : E_0, $\sigma_{0.2}$, $\sigma_{1.0}$, σ_U, and ε_u ,and n. The proposed model has been compared with classical models and indicates good accuracy in the full range stain-stress curve for austenitic stainless steel.

$$\varepsilon=\begin{cases}\dfrac{\sigma}{E_0}+0.002\left(\dfrac{\sigma}{\sigma_{0.2}}\right)^{n} & 0\le\sigma\le\sigma_{0.2}\\[2ex] \dfrac{\sigma}{E_0}+0.002\left(\dfrac{\sigma}{\sigma_{0.2}}\right)^{n_2} & \sigma_{0.2}<\sigma\le\sigma_{1.0}\\[2ex] \left(\dfrac{\sigma}{p}\right)^{q} & \sigma_{1.0}<\sigma\le\sigma_{u}\end{cases} \tag{3}$$

$$\begin{cases} n=\dfrac{\ln(20)}{\ln(\sigma_{0.2}/\sigma_{0.01})}, \qquad n_1=\dfrac{\ln(5)}{\ln(\sigma_{1.0}/\sigma_{0.2})}\\[2ex] n_2=n+\left(\dfrac{\sigma-\sigma_{0.2}}{\sigma_{1.0}-\sigma_{0.2}}\right)(n_1-n)\\[2ex] q=\dfrac{\ln(\varepsilon_u/\varepsilon_{1.0})}{\ln(\sigma_u/\sigma_{1.0})}, \quad p=\dfrac{\sigma_{1.0}}{\sqrt[q]{\varepsilon_{1.0}}}\end{cases} \tag{4}$$

4.2 Strength enhancement model for CHS

Several prediction models for nominal yield stress and ultimate stress of cold formed tube have been proposed [11-17] while part of these models were empirical formulas [11-15]. Rossi [16-17] developed a model for nominal yield stress by using a power law material model and average plastic strain. The nominal yield stress was obtained by taking the average plastic strain into the power law material model. In this paper, similar idea was employed. Equivalent strain was used instead of the average plastic strain, and was determined for each material parameter.

E_0

Comparison between the initial elastic modulus E_0 of the virgin plate and that of the cold formed tube shows that E_0 was almost the same for these two states. Thus, the initial elastic modulus E_0 of the cold formed tube is approximately equal to that of the virgin plate.

$\sigma_{0.2,cr,cir}$

A power law model was proposed for the nominal yield stress by trial and error, and is shown in Eq.(5). In Eq.5, $\sigma_{0.2,cr,cir}$ is the nominal yield stress of cold rolled CHS; ε_{eq} is the equivalent strain; t and R is the thickness and the radius of the cold rolled CHS, respectively; $\sigma_{0.2,v}$, $\sigma_{u,v}$, $\varepsilon_{u,v}$, and q are the material parameters of the virgin plate; α is a scale factor. When a plate was bent into a tube under a uniform moment, the plastic strain on the outer surface was $t/2R$. The equivalent strain for the nominal yield stress of cold rolled CHS was determined as half of the maximum plastic strain plus 0.01. The constant 0.01, also called reducing rate, represented the uniform compression in the transverse direction.

$$\begin{cases}\sigma_{0.2,cr,cir}=\sigma_{0.2,v}\left(1+\alpha\cdot\varepsilon_{eq}^{0.5}\right)\\[2ex] \alpha=\dfrac{1.5\left(\dfrac{q}{q+1}\sigma_{u,v}-\sigma_{0.2,v}\right)}{\sigma_{0.2,v}\cdot\sqrt{\varepsilon_{u,v}}}\\[2ex] \varepsilon_{eq}=\dfrac{1}{2}\dfrac{t}{2R}+0.01\end{cases} \tag{5}$$

$\sigma_{1.0,cr,cir}$

The prediction model for σ1.0 is shown in Eq.(6). In this equation, $\sigma_{1.0,cr,cir}$ is the stress with plastic strain 1%; p, and q are the material parameter of the virgin plate; $\varepsilon_{1.0,v}$ is the total strain when the stress is equal to $\sigma_{1.0}$ according to the stress-strain curve of virgin plate. $\sigma_{u,cr,cir}$ is the ultimate stress of the cold rolled CHS. For $\sigma_{1.0,cr,cir}$, the equivalent strain was determined as three quarters of the strain on the outer surface of the tube plus 0.01. According to the isotropic hardening assumption, the $\sigma_{1.0,cr,cir}$ was approximately equal to the stress corresponding to the strain (ε_{eq} +$\varepsilon_{1.0,v}$) on the stress-strain curve of virgin plate. The strain (ε_{eq} +$\varepsilon_{1.0,v}$) belongs to the third stage of material model. So the stress $\sigma_{1.0,cr,cir}$ can be easily obtained by taking (ε_{eq} +$\varepsilon_{1.0,v}$) into the third equation of Eq.(1). To increase the accuracy of prediction, an empirical factor (1-0.5 ε_{eq}^2) was used.

$$\begin{cases} \sigma_{1.0,cr,cir} = p \cdot \sqrt[q]{\varepsilon_{eq} + \varepsilon_{1.0,v}} \left(1 + 0.5\varepsilon_{eq}^2\right) \le \sigma_{u,cr,cir} \\ \varepsilon_{eq} = \dfrac{3}{4}\dfrac{t}{2R} + 0.01 \end{cases} \tag{6}$$

$\varepsilon_{u,cr,cir}$ and $\sigma_{u,cr,cir}$

The prediction model for $\varepsilon_{u,cr,cir}$ and $\sigma_{u,cr,cir}$ is shown in Eq. (7). In this equation, $\varepsilon_{u,cr,cir}$ and $\sigma_{u,cr,cir}$ is the ultimate strain and ultimate stress of the cold rolled CHS, respectively; $\varepsilon_{t,eq}$ is the equivalent strain; $\varepsilon_{t,u}$ and $\sigma_{t,u}$ is the real strain and the real stress at the ultimate state of the virgin plate, $\varepsilon_{t,u}$=ln(1+$\varepsilon_{u,v}$), $\sigma_{t,u}$= $\sigma_{u,v}$ (1+$\varepsilon_{u,v}$). For $\varepsilon_{u,cr,cir}$ and $\sigma_{u,cr,cir}$, the equivalent strain is three quarters of the real strain on the outside surface of the tube. According to the test data, the real stress at ultimate state $\sigma_{t,u}$ of the virgin material and that of the cold rolled tube are approximately the same. Similar situation occurs to the real strain at ultimate state $\varepsilon_{t,u}$. Provided the real strain during cold rolling, the $\varepsilon_{u,cr,cir}$ of the cold rolled CHS can be calculated using the first equation in Eq.(7) and the corresponding $\sigma_{u,cr,cir}$ can be calculated using the second equation in Eq.(7).

$$\begin{cases} \varepsilon_{u,cr,cir} = e^{\varepsilon_{t,u} - \varepsilon_{t,eq}} - 1 \\ \sigma_{u,cr,cir} = \dfrac{\sigma_{t,u}}{1 + \varepsilon_{u,cr,cir}} \\ \varepsilon_{t,eq} = \dfrac{3}{4}\ln\left(1 + \dfrac{t}{2R}\right) \end{cases} \tag{7}$$

$n_{cr,cir}$

Based on the available test data, the strain hardening exponent in the first stage of the material model is about 0.45 times of the exponent in the second stage. Thus, Eq.(8) was proposed for the strain hardening exponent of the first stage in the material model. In this equation, $n_{1,cr,cir}$ is the working hardening exponent of the second stage; $\sigma_{0.2,cr,cir}$ and $\sigma_{1.0,cr,cir}$ are the stress corresponding to 0.2% and 1.0% plastic strain according to the strain-stress curve of cold rolled CHS.

$$n_{cr,cir} = 0.45 n_{1,cr,cir} = 0.45 * \frac{\ln(5)}{\ln\left(\sigma_{1.0,cr,cir} / \sigma_{0.2,cr,cir}\right)} \tag{8}$$

4.3 Strength enhancement model for RHS

The strength enhancement model for RHS was like that of the CHS, except the equivalent strain.

Firstly, it was assumed that the plastic strain of the plate surface in the case of bending a plate into an arch shell of radius r_x, is equal to that in the case of flatting an arch shell with radius r_x into a plate. Thus, the total plastic strain experienced on the surface was t/r_x when the whole process is considered including forming an arch shell and flatting an arch shell. What is more, a reducing rate 0.005~0.02 was usually used to maintain the quality of product during crushing into a RHS. The equivalent strain for every material parameter can be obtained given the radius r_x. Take the nominal yield stress for example, the equivalent strain for the nominal yield stress was half the maximum plastic strain (t/r_x) plus 0.03.

Secondly, the parameter r_x should be determined for every point in the RHS. The parameter r_x was equal to the radius R of CHS for the centre of the flat face. And it is also clear that the parameter r_x was equal to the radius of the corner (r_o-t/2) for the point on the edge of the flat face. For points between the centre of the flat face and the edge of the flat face, r_x was interpolated between R and (r_o-t/2) according to the distance away from centre of the flat face.

Finally, Eq.(9)~Eq.(12) show the strength enhancement model for RHS. In these equations, $\sigma_{0.2,cr,f}$, $\sigma_{1.0,cr,f}$, $\varepsilon_{u,cr,f}$, $\sigma_{u,cr,f}$, and $n_{,cr,f}$ are material parameters of the flat face in RHS; $\sigma_{0.2,v}$, $\varepsilon_{1.0,v}$, $\varepsilon_{u,v}$, $\sigma_{u,v}$, p, and q are material parameters of virgin plate; $\varepsilon_{t,u}$ and $\sigma_{t,u}$ are the real strain and the real stress at the ultimate state of virgin plate; B, H, r_0 and R are geometric parameters defined in Fig.12.

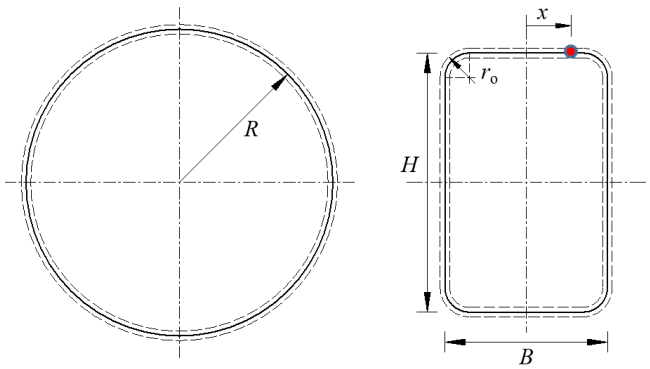

Fig. 12 Definition of geometric parameters used in Eq.(9) to Eq.(12)

$$\begin{cases} \sigma_{0.2,\mathrm{cr,f}} = \sigma_{0.2,\mathrm{v}}\left(1+\alpha\cdot\varepsilon_{\mathrm{eq}}^{0.5}\right) \\ \alpha = \dfrac{1.5\left(\dfrac{q}{q+1}\sigma_{\mathrm{u,v}} - \sigma_{0.2,v}\right)}{\sigma_{0.2,v}\cdot\sqrt{\varepsilon_{\mathrm{u,v}}}} \\ \varepsilon_{\mathrm{eq}} = \dfrac{1}{2}\dfrac{t}{r_x} + 0.03 \\ r_{\mathrm{x}} = \dfrac{2\pi R - 4\left(1+\dfrac{H}{B}\right)x}{2\pi} \end{cases} \tag{9}$$

$$\begin{cases} \sigma_{1.0,\mathrm{cr,f}} = p\cdot\sqrt[q]{\varepsilon_{\mathrm{eq}}+\varepsilon_{1.0,\mathrm{v}}}\left(1+0.5\varepsilon_{\mathrm{eq}}^{2}\right) \le \sigma_{\mathrm{u,cr,f}} \\ \varepsilon_{\mathrm{eq}} = \dfrac{3}{4}\dfrac{t}{r_{\mathrm{x}}} + 0.03 \end{cases} \tag{10}$$

$$\begin{cases} \varepsilon_{\mathrm{u,cr,f}} = e^{\varepsilon_{\mathrm{t,u}}-\varepsilon_{\mathrm{t,eq}}} - 1 \\ \sigma_{\mathrm{u,cr,f}} = \dfrac{\sigma_{\mathrm{t,u}}}{1+\varepsilon_{\mathrm{u,cr,f}}} \\ \varepsilon_{\mathrm{t,eq}} = \dfrac{3}{4}\ln\left(1+\dfrac{t}{r_{\mathrm{x}}}\right) \end{cases} \tag{11}$$

$$n_{\mathrm{cr,f}} = 0.45 n_{1,\mathrm{cr,f}} = 0.45 * \frac{\ln(5)}{\ln\left(\sigma_{1.0,\mathrm{cr,f}}/\sigma_{0.2,\mathrm{cr,f}}\right)} \tag{12}$$

4.4 Comparisons

All the material parameters were generated for each test coupon by using the prediction model proposed in this paper. The prediction models proposed by Rossi [17] and Cruise [15] were also used to calculate nominal yield stress and ultimate yield stress for each test coupon. Table 4 and Table 5 show the comparisons of the test data and the predictions for RHS 100mm×100mm×3mm and CHS 127mm×3mm, respectively.

Table 4 Comparison test material parameters with predictions proposed by this paper, Rossi, and Cruise for RHS100mm×100mm×3mm

Coupons	Test/Predict									
	This paper							Rossi	Cruise	
	x	r_x	σ_u	ε_u	$\sigma_{1.0}$	$\sigma_{0.2}$	n	$\sigma_{0.2}$	$\sigma_{0.2}$	σ_u
M100×3-2	40	11.41	0.97	1.21	1.02	1.01	0.84	1.28	1.60	1.07
M100×3-4	20	36.87	1.01	1.12	0.92	0.93	1.09	0.99	1.23	0.99
M100×3-6	2.5	59.15	1.02	1.03	0.97	0.98	1.03	0.99	1.24	0.98
M100×3-8	20	36.87	0.99	0.93	0.98	0.97	0.75	1.03	1.28	0.98
M100×3-10	40	11.41	1.01	1.18	1.13	1.05	0.65	1.33	1.65	1.12
M100×3-12	40	11.41	0.97	1.23	1.07	1.02	0.70	1.30	1.62	1.07
M100×3-14	20	36.87	-	-	1.09	1.11	0.98	1.18	1.47	-
M100×3-16	2.5	59.15	1.02	1.03	0.99	1.00	1.03	1.02	1.27	0.98
M100×3-18	20	36.87	-	-	0.92	0.93	1.04	0.98	1.23	-
M100×3-20	40	11.41	1.00	1.21	1.11	1.04	0.65	1.32	1.65	1.11
M100×3-22	40	11.41	0.98	1.10	1.10	0.96	0.49	1.22	1.52	1.08
M100×3-24	20	36.87	1.03	1.04	0.95	0.97	0.95	1.03	1.28	1.01
M100×3-26	2.5	59.15	1.02	1.05	0.97	0.96	0.81	0.98	1.22	0.98
M100×3-28	20	36.87	1.02	1.04	0.98	0.99	0.90	1.05	1.31	1.00
M100×3-30	40	11.41	1.03	1.21	1.13	1.02	0.55	1.29	1.61	1.14
M100×3-32	40	11.41	1.01	1.10	1.13	1.05	0.65	1.34	1.67	1.12
M100×3-34	20	36.87	-	-	0.90	0.92	0.99	0.97	1.21	-
M100×3-36	2.5	59.15	1.03	1.08	0.94	0.95	1.09	0.96	1.20	0.99
M100×3-38	20	36.87	-	-	0.93	0.94	1.00	1.00	1.24	-
M100×3-40	40	11.41	0.98	1.12	1.04	0.99	0.70	1.26	1.57	1.08
Avg.			1.00	1.10	1.01	0.99	0.85	1.13	1.40	1.04
Cov.			0.02	0.08	0.08	0.05	0.19	0.15	0.19	0.06
Max.			1.03	1.23	1.13	1.11	1.09	1.34	1.67	1.14
Min.			0.97	0.93	0.90	0.92	0.49	0.96	1.20	0.98

Table 5 Comparison test material parameters with predictions proposed by this paper, Rossi for CHS127mm×3mm

Coupons	Test/Predict					
	This paper					Rossi
	σ_u	ε_u	$\sigma_{1.0}$	$\sigma_{0.2}$	n	$\sigma_{0.2}$
M127×3-0	-	0.76	1.27	1.29	1.02	1.27
M127×3-60	1.00	1.03	0.91	0.90	1.16	0.88
M127×3-120	1.01	1.06	0.94	0.93	1.03	0.92
M127×3-180	-	1.03	1.08	1.09	1.06	1.08
M127×3-240	1.02	1.06	0.99	1.00	1.54	0.98
M127×3-300	1.01	0.99	0.95	0.96	1.27	0.94
Avg.	1.01	0.99	1.02	1.03	1.18	1.01
Cov.	0.01	0.11	0.13	0.15	0.20	0.14
Max.	1.02	1.06	1.27	1.29	1.54	1.27
Min.	1.00	0.76	0.91	0.90	1.02	0.88

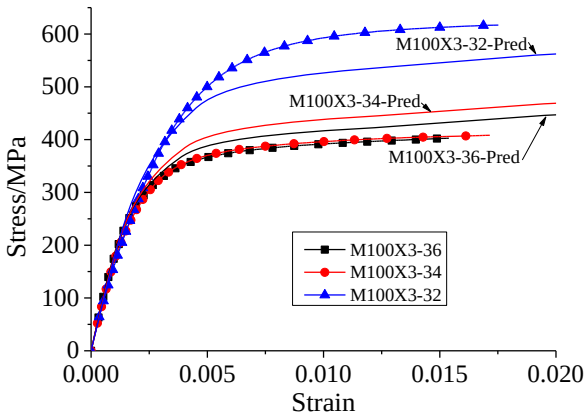

(a) RHS 100mm×100mm×3mm

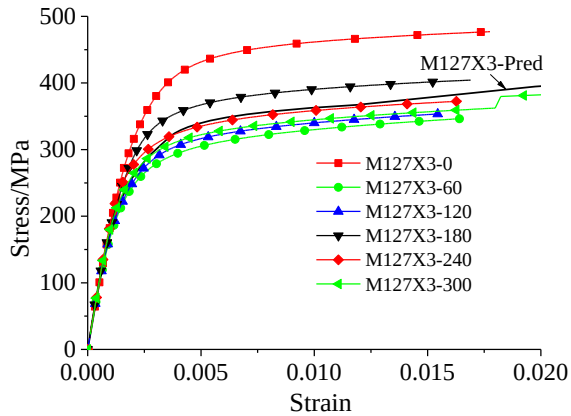

(b) CHS 127mm×3mm

Fig. 13 Comparison the test stress-strain curve with the predicted stress-strain curve-the initial stage

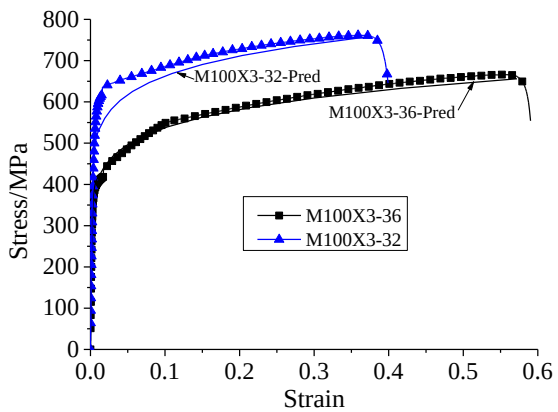

Fig. 14 Comparison the test stress-strain curve with the predicted stress-strain curve-the full range

Table 4indicates that: (1) the predictions by the proposed material model agreed well the test material parameters. The mean ratio of test data over the predictions for $\sigma_{0.2}$, $\sigma_{1.0}$, ε_u,and $\sigma_{u,v}$ were 0.99, 1.01, 1.10 , and 1.00, respectively. For the strain hardening exponent n, the prediction model did not give accurate results with the average ratio of test value over

the predictions at 0.89 with a large scatter 0.19. (2) Both the prediction models proposed by Rossi [17] and Cruise [15] gave conservative predictions for the nominal yield stress, with mean ratio of test data over the predictions at 1.13 and 1.40, respectively. In these two models, the nominal yield stress was assumed to be constant along the flat face of the cold rolled RHS that was different from the test observations. That is the main reason for the conservative prediction. (3)The ultimate stress predicted using Cruise's model agreed well with the test data. The mean ratio of the test data over the predictions was 1.04, with a low scatter of 0.06.

Table 5 shows that: (1) the predictions calculated by the proposed model matched well with the test material data. The mean ratio of test data over the predictions for $\sigma_{0.2}$, $\sigma_{1.0}$, ε_u,and $\sigma_{u,v}$ were 1.03, 1.02, 0.99 and 1.01, respectively. However, the scatters of these predictions for CHS was larger than those for RHS because the material (M127×3-0) used for the CHS coupon has higher nominal yield stress and ultimate stress than the other coupons that is not applicable for the proposed model. (2) The predictions calculated using Rossi's model indicate good agreement with test data. The mean ratio of the test data over the predictions was 1.01. The model proposed by Rossi and in this paper show similar accuracy in predicting the nominal yield stress of CHS.

Fig. 13 shows the comparison of the initial stage of test stress-strain curve with the predicted stress-strain curve while Fig. 14 shows the comparison of the full range of test stress-strain curve with the predicted stress-strain curve. It is observed that the predicted stress-strain curve can represent the test stress-strain curve with an acceptable accuracy.

5 Conclusions

(1) Residual stresses were measured for four circular and four rectangular cold rolled hollow sections. Longitudinal bending residual stresses and transverse bending residual stresses were observed to be the dominate types of residual stress in cold rolled members. Based on the test data, the distribution models of residual stress were proposed for circular and rectangular hollow sections, respectively.

(2) Material tensile tests were performed for both the virgin plates and the cold rolling members. Considerable strength enhancement was observed in the test data. For RHS, the material yield stress was increased gradually from the centre region of the flat surface to the corner of the cross section. For CHS, the coupons cut from on the weld had much higher yield stress than that from other regions.

(3) Strength enhancement models for RHS and CHS were proposed, respectively for the predication of the full material parameters in the cold rolled stainless steel members. The proposed model indicates good accuracy through comparisons with the test data.

Acknowledgements

The research work described in this paper is supported by the Priority Academic Program Development of Jiangsu Higher Education Institutions and by the National Science Foundation of China through the projects No. 51378105 and 51578134. The financial support is highly appreciated. Special thanks to the Jiangsu Dongge Stainless steel Ware Co., Ltd. for providing the test specimens.

References

[1] Rasmussen K.J.R., Hancock G.J. Design of cold-formed stainless steel tubular members. I: columns. Journal of Structural Engineering, ASCE, 1993, 119(8): 2349-2367.

[2] Quach W.M., Teng L.G., Chung K.F. Residual stresses in press-braked stainless steel sections, I: coiling and uncoiling of sheets. Journal of Constructional Steel Research, 2009, 65: 1803-1815.

[3] Quach W.M., Teng L.G., Chung K.F. Residual stresses in press-braked stainless steel sections, II: Press-braking. Journal of Constructional Steel Research, 2009, 65: 1816-1826.

[4] Young B., Liu W.M. Behavior of cold-formed high strength stainless steel sections. Journal of Structural Engineering, 2005, 131(11): 1738-1745.

[5] Cruise R.B., Gardner L. Residual stress analysis of structural stainless steel sections. Journal of Constructional Steel Research, 2008, 64: 352-366.

[6] Gardner L., Cruise R.B. Modeling of residual stresses in structural stainless steel sections. Journal of Structural Engineering, 2009, 135(1): 42-53.

[7] Jandera M., Gardner L. and Machacek J. Residual stresses in cold-rolled stainless steel hollow sections. Journal of Constructional Steel Research, 2008, 64: 1255-1263.

[8] Jandera M., Machacek J. Residual stress pattern of stainless steel SHS. *Tubular Structures XII*, 2010, 265.

[9] Huang Y., Young B. Material properties of cold-formed lean duplex stainless steel sections. Thin-Walled Structures, 2012, 54: 72-81.

[10] Bredenkamp P.J., van den Berg G.J., van der Merwe P. Residual stresses and the strength of stainless steel I-section columns. In: Proceedings of the structural stability research council, Annual technical session, 1992: 69-86.

[11] Coetsee J.S., Van den Berg G.J., Van der Merwe P. The effect of work hardening and residual stresses due to cold work of forming on the strength of cold-formed stainless steel lipped channel sections. Tenth international specialty conference on cold formed steel structures, St. Louis, Missouri, U.S.A., October 23-24, 1990.

[12] Gardner L. A new approach to stainless steel structural design. PhD Thesis. Structures Section. Department of Civil and Environmental Engineering, Imperial College, London, 2002.

[13] Gardner L. The use of stainless steel in structures. Review Article. Steel Construction, 2005, 7: 45-55.

[14] Ashraf M., Gardner L., and Nethercot D.A. Strength enhancement of the corner region of stainless steel cross-sections. Journal of Constructional Steel Research, 2005, 61:37-52.

[15] Cruise R.B., Gardner L. Strength enhancements induced during cold forming of stainless steel sections. Journal of Constructional Steel Research 2008; 64(11):1310-6.

[16] Afshan S., Rossi B., Gardner L. Strength enhancements in cold-formed structural sections − part I: material testing. Journal of Constructional Steel Research, 2013, 83:177-88.

[17] Rossi B., Afshan S., Gardner L. Strength enhancements in cold-formed structural sections − Part II: Predictive models. Journal of Constructional Steel Research s, 2013, 83:189-96.

[18] Quach W.M., Qiu P. Strength and ductility of corner materials in cold-formed stainless steel sections. Thin-Walled Structures, 2014, 83:28–42.

[19] Lagerqvist O., Olsson A. Residual stresses in welded I-girders made of stainless steel and structural steel. In: Proceedings of the 9th Nordic steel construction conference, 2001, 737-744.

[20] Wang Y.Q., Guan J., Zhang Y., Shi Y.J., Yang L. Experimental study on residual stress of austenitic stainless steel 316 in fabricated I-sections. Industrial Construction, 2012,42(5): 44-50. (in Chinese)

[21] Yuan H.X., Wang Y.Q., Shi Y.J, and Gardner L. Residual stress distributions in welded stainless steel sections. Thin-Walled Structures, 2014, 79: 38-51.

[22] Schajer G.S. Practical residual stress measurement methods. John Wiley & Sons, United Kingdom, 2013.

[23] Halmos G.T. Roll Forming Handbook. Taylor & Francis, 2005.

[24] Tebedge N., Alpten G., and Tall L. Residual-stress measurement by the sectioning method. Experimental Mechanics, 1973, 13(2): 88-96.

[25] GB/T 228.1-2010. Metallic materials-tensile testing-Part 1: Method of test at room temperature. China Standard Press, Beijing, 2010 (in Chinese).

[26] Ramberg W., Osgood W.R. Description of stress-strain curves by three parameters. Technical Note, No.902. National Advisory Committee for Aeronautics. Washington DC: 1943.

[27] Macdonald M., Rhodes J., Taylor G.T. Mechanical properties of stainless steel lipped channels. Proc. 15th Int. Specialty Conf. on Cold-Formed Steel Structures, University of Missouri-Rolla, Mo. 673–686.

[28] Olsson A. Stainless steel plasticity-Material modelling and structural applications, Ph.D. thesis, Division of Steel Structures, Dept. of Civil and Mining Engineering, Luleå Univ. of Technology, Sweden.

[29] Mirambell E., and Real E. On the calculation of deflections in structural stainless steel beams: An experimental and numerical investigation. Journal of Constructional Steel Research, 2000, 54:109–133.

[30] Rasmussen K. J. R. Full-range stress-strain curves for stainless steel alloys. Journal of Constructional Steel Research. 2003, 59:47-61.

[31] Quach W.M., Teng J.G., Chung K.F. The-stage full-range stress-stain model for stainless steel. Journal of Structural Engineering, 2008, 134(9):1518-1527.